Static Synchronous Generator Model: A New Perspective to Investigate Dynamic Characteristics and Stability Issues of Grid-Tied PWM Inverter

Liansong Xiong, *Student Member, IEEE*, Fang Zhuo, *Member, IEEE*, Feng Wang, *Member, IEEE*, Xiaokang Liu, Ying Chen, Minghua Zhu, and Hao Yi, *Member, IEEE*

***Abstract*—With increasing penetration of the renewable energy, the grid-tied PWM inverters need to take corresponding responsibilities for the security and stability of future grid, behaving like conventional rotational synchronous generator (RSG). Therefore, recognizing the inherent relationship and intrinsic differences between inverters and RSGs is essential for such target. By modeling the typical electromechanical transient of grid-tied PWM inverters, this paper first proves that PWM inverters and RSGs are similar in physical mechanism and equivalent in mathematical model, and the concept of static synchronous generator (SSG) is thereby developed. Furthermore, the comprehensive comparison between RSG and SSG is carried out in detail, and their inherent relation is built. Based on these findings, the rationality and feasibility of migrating the concepts, tools, and methods of RSG stability analysis to investigate the dynamic behaviors and stability issues of SSG is therefore confirmed. Taking stability issues as an example, the criteria of small signal and transient stability of a typical grid-tied PWM inverter is put forward to demonstrate the significance of the developed SSG model (including synchronizing coefficient, damping coefficient, inertia constant, and power-angle curve), providing clear physical interpretation on the dynamic characteristics and stability issues. The developed SSG model promotes grid-friendly integration of renewable energy to future grid and stimulates interdisciplinary research between power electronics and power system.**

***Index Terms*—Inherent relation, renewable energy power generation, rotational synchronous generator, small-signal stability, static synchronous generator, transient stability.**

I. Introduction

INTERMITTENT energy sources such as wind and solar power often use pulse-width modulation (PWM) inverters as the interface circuit to achieve grid-tied power generation [1]–[5]. The PWM inverters are analogous to the rotational synchronous generators (RSGs) in traditional power generation, yet their energy transfer media are different, i.e., conventional generators convert the mechanical power of prime movers to the electromagnetic power of RSG through its rotor's rotational kinetic energy, while the energy medium of inverter-based generation systems is the static capacitor, which achieves the power balancing between prime movers (wind, solar, etc.) and grid-tied inverters by charging and discharging. In this sense, the grid-tied PWM inverters and RSGs, which are distinguished mainly through the mechanical behaviors, i.e., static or rotational, play an equal role in their respective system, and the behaviors of their energy transfer media can be described by the same fist-order kinetic equation [6], [7]. Furthermore, both of their normal operation must be synchronized with grid. Accordingly, the grid-tied PWM inverter is referred to as static synchronous generator (SSG) in this paper, and hence, the concept of synchronous generator (SG) are expanded to RSG and SSG. What should be mentioned in advance is that the dynamic behaviors and stability issues of grid-tied inverters can be comprehended clearly and easily by the developed SSG model and, therefore, the basic idea and main purpose of the SSG model is completely different to that of the popular virtual synchronous generator (VSG) technology.

SSG is the core equipment of renewable energy generation system, and its safety and stability affect the reliability of entire system [8]–[17]. Existing methods for SSG stability analysis mainly comprise of the time-domain simulation method [8]–[10], eigenvalue analysis [11]–[15], and impedance analysis [16]–[21]. The simulation method illustrates intuitively the dynamic characteristics of SSG in time domain [8]–[10], thus, the harmonic analysis, controller design, short-circuit current calculation, and relay protection verification in a specific SSG can be achieved [9]. However, the instability mechanism behind a system cannot be readily analyzed, meanwhile the conclusions obtained for a specific application are not necessarily universally applicable for other systems [10]. Eigenvalue analysis establishes differential equations for the whole inverter system and uses the eigenvalue theory to analyze the system stability [11]–[15]; however, the order of differential equations increases dramatically as the system complexity increases [12]–[14]. Accordingly, when this method is applied to the dynamic behavior analysis of a multiinverter system, the dynamic stability and the physical mechanism cannot be recognized easily because the high-order mathematical model can hardly show the clear physical meaning of the system [13], [14], resulting in great inconvenience to achieve the best design and optimal control [15]. Impedance analysis method is based on the concept of stability forbidden region [16], [17], and its application to dc system stability analysis is a great success. In the case of ac systems, however, many theoretical and technical problems are still unsolved

Manuscript received June 25, 2015; revised September 15, 2015; accepted October 25, 2015.

The authors are with the State Key Laboratory of Electrical Insulation and Power Equipment, Xi'an Jiaotong University, Xi'an 710049, China (e-mail: xiongliansong@163.com; zffz@mail.xjtu.edu.cn; fengwangee@xjtu.edu.cn; mrliuemail@163.com; ying.zc.g@gmail.com; yzmhxjtu@gmail.com; yi_hao@xjtu.edu.cn).

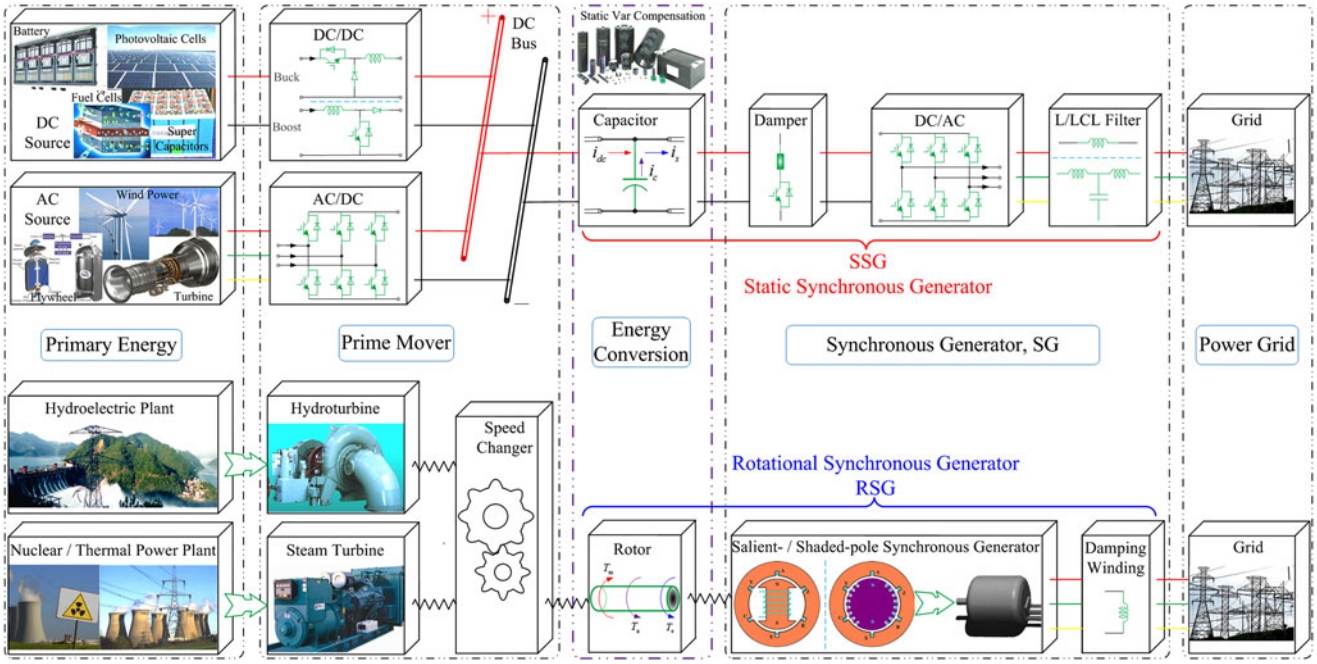

Fig. 1. Generalized structure of renewable/conventional energy generation system.

[18]–[21], and it is difficult to obtain a breakthrough in short term. In addition, the physical mechanism of instability of SSG can hardly be explained as well.

SSGs in renewable energy generation systems are mostly regulated as current sources [22]–[30], such that the renewable power can be adequately utilized. To this end, conventional SSGs are incapable of regulating their terminal voltage and frequency or the output power, meanwhile the autobalance, droop, and inertia characteristics of RSGs are not retained for present SSGs [22]–[26], leading to potential problems of grid utility in safe operation. With the increasing penetration level of renewable power, the irresponsible operation of SSG cannot meet the requirement of safe and stable operation of future grid. Consequently, technical improvements need to be made for grid-tied SSGs to cooperate in the aspects of grid power balance, voltage/frequency regulation, fault ride-through control, and so on [6], [24]. For this purpose, the VSG technology is proposed [6]–[7], [22]–[30], aiming to mimic the RSG operating characteristics for SSGs through control methods. Several methods are developed accordingly, such as synchronverters [6], virtual synchronous machine [29], [30], virtual inertia control [22], [24] and the global dc-link voltage-based droop control [31]. However, there is a lack of sufficient demonstration that SSGs are able to mimic RSGs from the mathematical viewpoint in present studies, meanwhile the inherent relationship and intrinsic differences between SSG and RSG are not analyzed deeply from a theoretical perspective, which is essential for demonstrating the rationality and feasibility of migrating the concepts, tools and methods of RSG stability analysis to investigate the stability issues of SSG.

In this paper, several physical concepts related to an SSG are developed and analyzed by both mathematical models and physical mechanisms, demonstrating the inherent unity of SSG and RSG in physical meaning and internal mechanism, thus, proving the feasibility of VSG technology. In this sense, it is feasible to migrate the concepts, tools, and methods of RSG stability analysis to SSG applications. Based on this conclusion, the virtual swing equation, which describes the electromechanical process of an SSG, is developed in this paper and harnessed to analyze the small-signal/transient stability, providing a new methodology to analyze the dynamic behavior and stability of SSG. The well-developed theories and methods in conventional grid can be applied to SSGs based on this new methodology, promoting the unity of RSG and SSG in theories, methods, and tools, which is significant for investigating dynamic behaviors and stability issues of future RSG/SSG hybrid grid.

In this sense, the SSG model is beneficial for the clear cognizing of grid-tied inverters, as well as analyzing and designing the control strategies of SSGs from the perspective of grid safety and stability, effectively linking the gap between grid-tied inverter systems and conventional power systems. Therefore, the developed SSG model can bridge power electronics and power system, promoting the grid-friendly integration of renewable energy to future grid.

II. Configuration and Control of Grid-Tied Inverters in Renewable Energy Power Generation

A. General Configuration of Renewable Energy Power Generation Based on Grid-Tied Inverters

Generally, a renewable energy generation system (see Fig. 1) comprise of the primary energy source, the prime mover, the dc-side capacitor, the damper, the grid-tied inverter, the passive filter, and grid. The primary energy source mainly consists of wind power, solar power, chemical energy (such as batteries, super capacitors, and fuel cells) and mechanical power (e.g., energy stored in flywheel). The prime mover usually takes the

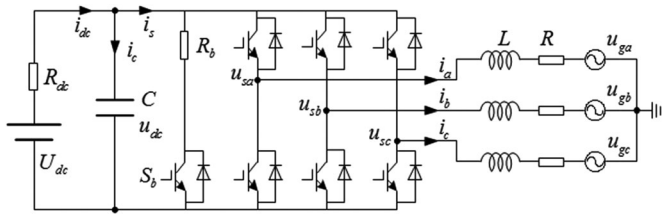

Fig. 2. Topology of SSG with an L-type filter.

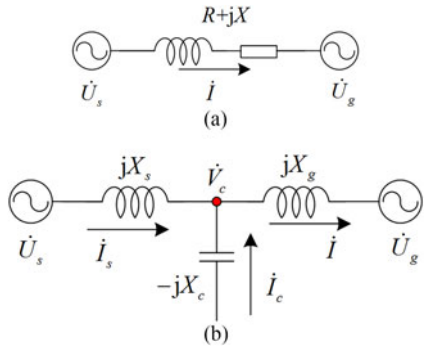

Fig. 3. Equivalent circuits of SSG with (a) L-type and (b) LCL-type filter.

form of dc/dc [32] or ac/dc converter. The damper circuit, which is also referred to as chopper circuit, is utilized to limit the dc voltage to a safety region. The grid-tied inverter can be the bridge inverter, diode-clamped/flying-capacitor inverter, modular multilevel converter, and so on.

By analyzing the structure of inverter-based generation system, it is apparent that the prime mover may differ for different primary energy and application. The prime mover can even be omitted in some specific applications such as photovoltaic generation, battery/super capacitor generation, and static VAR compensator. However, for any kind of renewable energy generation system, four components, i.e., the dc-side capacitor, the damper, the grid-tied inverter, and the passive filter are necessary to form the basic structure of the SSG. In addition, the diverse inverters are identical in major functions and can be represented by an ideal PWM bridge inverter (see Fig. 2) on the electromechanical time scale. Hence, the bridge inverter is utilized to describe the developed SSG model in this paper. R_b and S_b constitute the damper circuit (the counterpart of damping winding in RSG).

Generally, the PWM inverter is characterized by high (equivalent) switching frequency, hence, the harmonics of output current I are limited and have virtually no effect on the energy conversion process. In this sense, SSG can be simplified by taking into account only the fundamental component when the electromechanical transient is studied. In Fig. 3, the internal voltage U_S corresponds to the field voltage of RSG and the output voltage (fundamental component) of SSG; the terminal voltage of SSG U_g is also the grid voltage in this case; and the equivalent resistance R and inductance L ($X = \omega L$) are coherent with the stator inductor in RSG and the linking inductor in SSG (i.e., the passive filter corresponds with the stator circuit).

Neglecting R, the phasor diagram of SSG with L-type filter can be obtained as shown in Fig. 4(a). It is noted that the q-axis is aligned with U_S in this case such that the comparison between

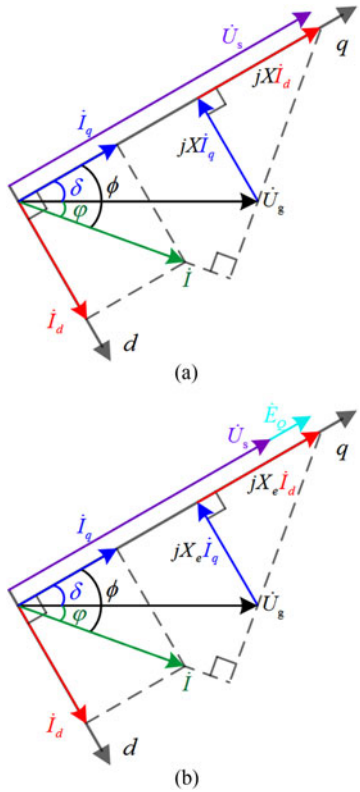

Fig. 4. Phasor diagrams of SSGs with (a) L-type and (b) LCL-type filter.

RSG and SSG can be readily performed. In general cases of grid-tied inverter modeling, the d-axis is often aligned with U_g.

The output power of SSG with L-type filter, according to Fig. 4(a), can be obtained as

$$P_\mathrm{e} = P_\mathrm{max} \sin\delta = \frac{3}{2}\frac{U_\mathrm{s}U_\mathrm{g}}{X}\sin\delta \tag{1}$$

$$Q_\mathrm{e} = \frac{3}{2}\frac{U_\mathrm{g}\left(U_\mathrm{s}\cos\delta - U_\mathrm{g}\right)}{X}. \tag{2}$$

According to Fig. 4(a) and (1), (2), the phasor diagram and output power of SSG with L-type filter are counterparts of the shaded-pole RSG. Similarly, the SSG with LCL-type filter corresponds to the salient-pole RSG.

B. Equivalence of SSG With L- and LCL-Type Filters on Electromechanical Time Scale

The equivalent circuit and phasor diagram of the SSG with LCL-type filter, neglecting R, can be obtained as shown in Figs. 3(b) and 4(b), respectively. According to Kirchhoff's laws, the voltage and current phasors yield

$$\dot{U}_\mathrm{s} = \dot{V}_\mathrm{c} + jX_\mathrm{s}\dot{I}_\mathrm{s} \tag{3}$$

$$\dot{V}_\mathrm{c} = jX_\mathrm{c}\dot{I}_\mathrm{c} \tag{4}$$

$$\dot{V}_\mathrm{c} = \dot{U}_\mathrm{g} + jX_\mathrm{g}\dot{I} \tag{5}$$

$$\dot{I} = \dot{I}_\mathrm{s} + \dot{I}_\mathrm{c} \tag{6}$$

where, V_c is the capacitor voltage of LCL filter.

By combining (3) and (6), we have

$$\dot{U}_{\mathrm{g}} = k\dot{U}_{\mathrm{s}} - jX_e\dot{I} \tag{7}$$

where

$$k = \frac{X_{\mathrm{c}}}{X_{\mathrm{c}} - X_{\mathrm{s}}} \geq 1 \tag{8}$$

$$X_e = kX_{\mathrm{s}} + X_{\mathrm{g}}. \tag{9}$$

Generally, the capacitors in an LCL filter are several microfarads (μF) and the inductors are in the range of mH, hence $X_{\mathrm{c}} \gg X_{\mathrm{s}}$ and k is usually slightly larger than 1.

By aligning the q-axis with U_{S} [see Fig. 4(b)] and defining the virtual internal voltage of SSG with LCL-type filter as

$$\dot{E}_{\mathrm{Q}} = k\dot{U}_{\mathrm{s}}. \tag{10}$$

Then (7) can be rewritten as

$$\dot{U}_{\mathrm{g}} = k\dot{U}_{\mathrm{s}} - jX_e\dot{I} = \dot{E}_{\mathrm{Q}} - jX_e\dot{I}_{\mathrm{d}} - jX_e\dot{I}_{\mathrm{q}}. \tag{11}$$

According to Fig. 4(b), it is

$$\begin{cases} X_e I_{\mathrm{d}} = E_{\mathrm{Q}} - U_{\mathrm{g}}\cos\delta \\ X_e I_{\mathrm{q}} = U_{\mathrm{g}}\sin\delta. \end{cases} \tag{12}$$

By defining X as

$$X = \frac{X_e}{k} = X_{\mathrm{s}} + X_{\mathrm{g}} - \frac{X_{\mathrm{s}}X_{\mathrm{g}}}{X_{\mathrm{c}}} \tag{13}$$

the output electromagnetic power of SSG with LCL-type filter can be obtained as

$$\begin{aligned} P_e &= \frac{3}{2}U_{\mathrm{g}}I\cos\varphi = \frac{3}{2}U_{\mathrm{g}}I\cos(\phi - \delta) \\ &= \frac{3}{2}U_{\mathrm{g}}I_{\mathrm{q}}\cos\delta + \frac{3}{2}U_{\mathrm{g}}I_{\mathrm{d}}\sin\delta \\ &= \frac{3}{2}\frac{E_{\mathrm{Q}}U_{\mathrm{g}}}{X_e}\sin\delta = \frac{3}{2}\frac{U_{\mathrm{s}}U_{\mathrm{g}}}{X}\sin\delta. \end{aligned} \tag{14}$$

From Fig. 4(b) and (14), it is evident that SSG with LCL-type filter corresponds to the salient-pole RSG from the viewpoint of internal voltage and phasor relationship. Hence, the SSG with L- and LCL-type filters are counterparts of the shaded-pole and salient-pole RSGs, respectively.

Shaded-pole RSGs are characterized by the uniform distribution of poles as well as magnetic field along the periphery of the machine, and are generally applied to applications with higher rotational speed (e.g., in thermal power generation). SSGs with L-type filter, in which multilevel structure is generally applied, are characterized by high equivalent switching frequency and low harmonics, hence, they are widely applied in offshore wind power generation and flexible dc transmission. Salient-pole RSGs are harnessed to applications with low rotational speed such as hydraulic power generation, and the counterpart, SSG with LCL-type filter, is applied in power generation of distribution network with bridge inverters.

It is apparent from Fig. 4 that SSGs with L- and LCL-type filters are equivalent on the electromechanical time scale, furthermore the physical quantities are corresponding and the expressions of electromagnetic power are the same. Accordingly, SSG with L-type filter is analyzed in this paper as a generic case.

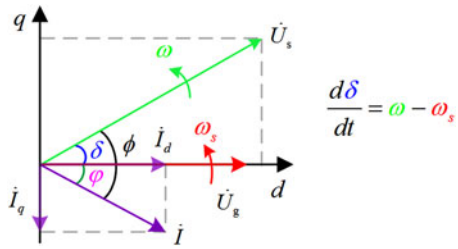

Fig. 5. Phasor diagram of a SSG when d-axis is aligned with grid voltage vector.

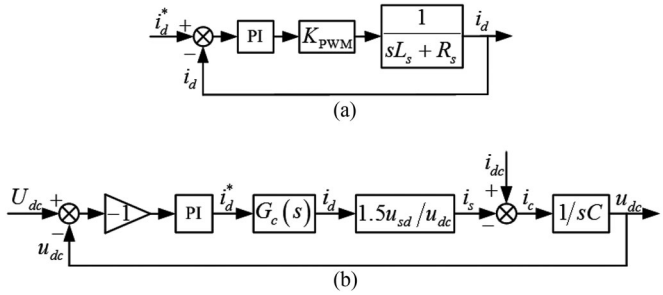

Fig. 6. Block diagrams of (a) inner loop current control and (b) outer loop voltage control.

C. Foundation Control Strategy of SSG

As a typical inverter modeling process, the d-axis is aligned with grid voltage vector [3], as shown in Fig. 5. The typical control (see Fig. 6) forms the foundation control framework of grid-tied inverter, under which SSG is able to be tied to the grid and generate electricity stably [1], [3].

From the analysis below, the stability of the SSG electromechanical process is mainly dependent on the dynamic behavior of dc-side capacitor, i.e., capacitor power balance ensures the stability of SSG, which is usually achieved by Fig. 6(b). Considering external disturbance, additional control strategies need to be implemented such that high performance control of dc capacitor voltage can be achieved. These additional control schemes, from the perspective of abnormal grid conditions, include abnormal grid voltage ride through, virtual inertia control, virtual damping control, and so on. If viewed from the disturbance of primary energy source, the control schemes consist of power fluctuation stabilization control, maximum power point tracking, primary/secondary frequency control, and so on. Whichever control scheme must help to realize power balance and capacitor voltage stability. Hence, the electromechanical dynamic is the key point to investigate the SSG stability. Furthermore, the fundamental control scheme illustrated in Fig. 6 is served as the basis of deducting the electromechanical model of SSG, thus analyzing the inherent relationship between SSG and RSG as well as identifying the electromechanical stability of SSG.

III. Inherent Relationship Between RSG and SSG

RSG and SSG share strong similarities in dimensions of physical structures, characteristic parameters, energy transfer

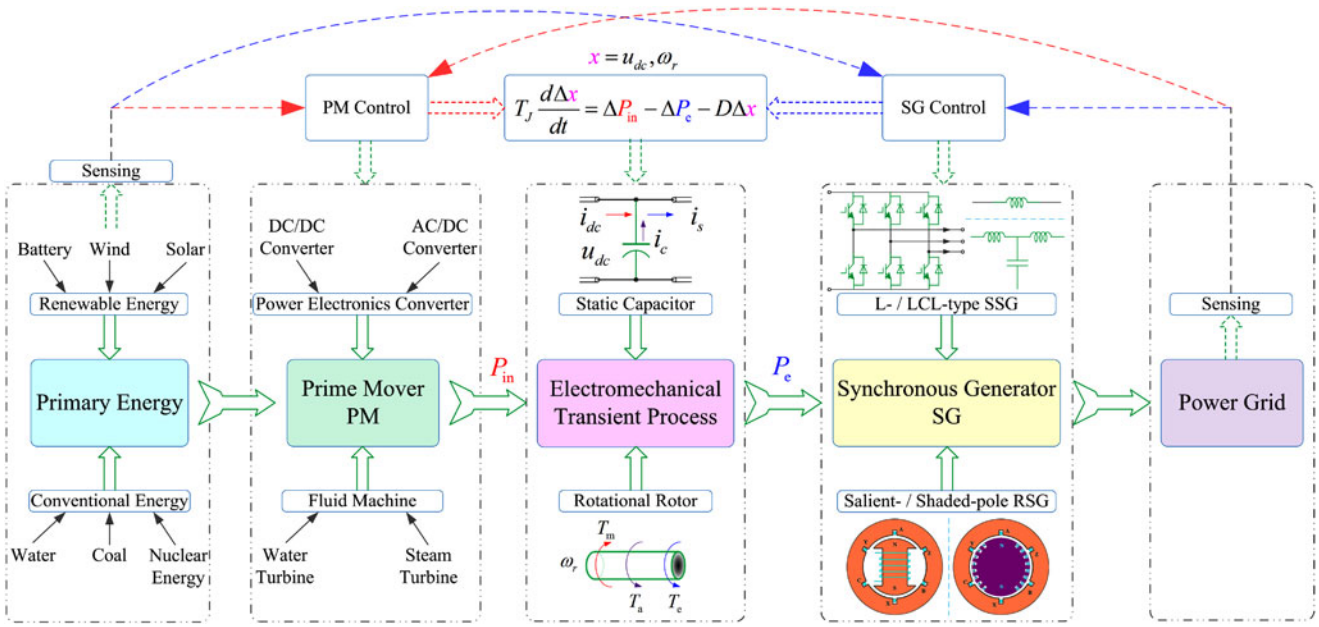

Fig. 7. Inherent relationship between SSG and RSG system in physical structure.

TABLE I
CORRESPONDENCE OF SSG/RSG SYSTEM COMPONENTS

	SSG	RSG
Primary Energy	Renewable Energy, Battery, Wind, Solar, etc.	Conventional Energy, Water, Coal, Nucleus, etc
Prime Mover, PM	Power Electronics Converter: dc/dc, ac/dc	Fluid Machine: Water Turbine, Steam Turbine
Energy Transfer Medium	Static Capacitor	Rotational Rotor
Damper	Chopper Circuit (IGBT + Power Resistor)	Damping Winding
Synchronous Generator	L-type SSG	Shaded-pole RSG
SG	LCL-type SSG	Salient-pole RSG

process, dynamic behaviors, and mathematical models, and goes as follows.

A. Inherent Similarity in Physical Structure

It is apparent from Fig. 1 that physical structures of conventional and renewable energy generation systems, which consist of the primary energy, the prime mover, the energy transfer medium, the SG, damper(s) and grid, are coherent (see Fig. 7). The physical structures of RSG and SSG are corresponding (see Table I). Besides, as a special application of SSG, the static VAR compensator is coherent with dynamic condenser (a special application of RSG) in the aspects of basic structure, working principle, major functions, and so on.

B. Correspondence of Characteristic Parameters

The characteristic parameters of SSG and RSG are also coherent, as shown in Table II [6], [7], [23], [25], [28], [30], and [31]. Besides, several key parameters that are not mentioned in present studies are compared and analyzed in this paper.

The moment of inertia J of the rotor in RSG, and the capacitance (assuming the parallel-plate capacitor) in SSG, are given by

$$\begin{cases} J = \dfrac{1}{2} m R^2 \\ C = \varepsilon_{\mathrm{r}} \varepsilon_0 \dfrac{A}{d} \end{cases} \tag{15}$$

where, m and R are the rotor mass and the radius of RSG, respectively; ε_{r}, A and d are the relative permittivity of the material between the plates, plate surface area and separation in SSG, respectively; ε_0 is the electric constant.

It is evident that J and C are independent of the rest parts of the two devices, i.e., they are free from the operation of SG. J is determined merely by the rotor structure and has no relation with the state or rotor speed; similarly, C is fixed regardless of the charges inside. Therefore, the increased inertia of grid-tied inverter based on VSG technology belongs to virtual inertia instead of intrinsic inertia of SSG. According to classical power system theory, the inertia consists of two parts (see Fig. 8): intrinsic inertia, which cannot be changed and depends on its intrinsic property, and virtual inertia that can be virtually constructed. The virtual inertia may come from control strategies (e.g., VSG technology [27], virtual inertia control [24]) and/or extra power (e.g., energy storage device [26], prime mover [22]). And so goes the damping effects.

TABLE II
CORRESPONDENCE OF SSG AND RSG IN CHARACTERISTIC PARAMETERS

SSG	RSG
Capacitance of Capaitor C	Moment of Inertia J
Passive Filter	Stator Circuit
DC Capacitor Voltage	Rotor Angle (P Controller) / Rotational Speed (I Controller)
Output Voltage of Inverter	Internal Voltage of RSG
Virtual Internal Voltage of SSG with LCL-type Filter	Virtual Internal Voltage of Salient-pole RSG
Output Voltage of Passive Filter	Terminal Voltage of RSG
Stored Electric Energy of Capacitor E_{K}	Rotational Kinetic Energy of Rotor W_{K}
Rated DC Capacitor Voltage	Synchronous Speed of Rotor
Input/Output/Charging Current of dc-side Capacitor	Mechanical/Electromagnetic/Accelerating Torque of Rotor

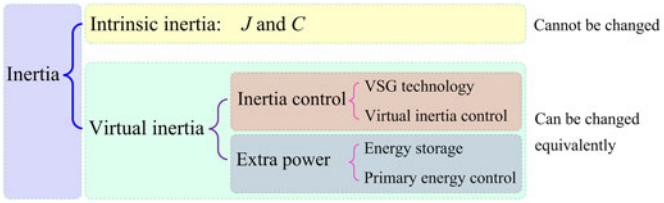

Fig. 8. Sources of inertia in SG systems.

From the energy transfer standpoint, rotor and capacitor work as power transmitters that transfer the input power to output.

The stored kinetic energy W_{K} at the synchronous rotor speed of RSG and the stored capacitor energy E_{K} of SSG are

$$\begin{cases} W_{\mathrm{K}} = \dfrac{1}{2} J \Omega_0^2 \\ E_{\mathrm{K}} = \dfrac{1}{2} C U_{\mathrm{dc}}^2 \end{cases} \tag{16}$$

where, Ω_0 is the synchronous rotor speed (in rd/s) of RSG, and U_{dc} the rated dc capacitor voltage (in V) of SSG.

It can be readily seen that the two types of energy, i.e., W_{K} and E_{K} are corresponding, and Ω_0 in RSG is coherent with U_{dc}.

C. Similarity of the Energy Transfer Process and Its Mathematical Model

The similarity between RSG and SSG can also be viewed by energy transfer process (i.e., electromechanical dynamic process) and the corresponding mathematical model.

The mechanical dynamic process in RSG and the current flow of the dc-side in SSG can be respectively described by

$$T_{\mathrm{a}} = J \frac{d\Omega}{dt} = T_{\mathrm{in}} - T_{\mathrm{e}} \tag{17}$$

$$i_{\mathrm{c}} = C \frac{du_{\mathrm{dc}}}{dt} = i_{\mathrm{dc}} - i_{\mathrm{s}} \tag{18}$$

where T_{in}, T_{e}, and T_{a} are the mechanical, electromagnetic, and accelerating torque of the rotor, respectively. Ω is the rotational speed. i_{dc}, i_{s}, and i_{c} are the input, output, and charging currents of the dc-side capacitor. u_{dc} is the dc capacitor voltage.

Considering the damping effect of chopper circuit, (18) should be revised as

$$i_{\mathrm{c}} = C \frac{du_{\mathrm{dc}}}{dt} = i_{\mathrm{dc}} - i_{\mathrm{s}} - i_{\mathrm{d}} = i_{\mathrm{dc}} - i_{\mathrm{s}} - \frac{u_{\mathrm{dc}}}{R_{\mathrm{d}}}. \tag{19}$$

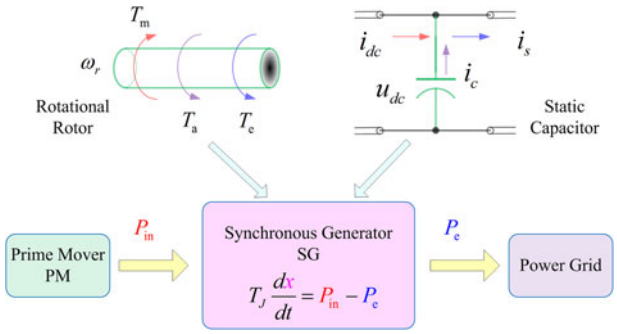

Fig. 9. Electromechanical transient process.

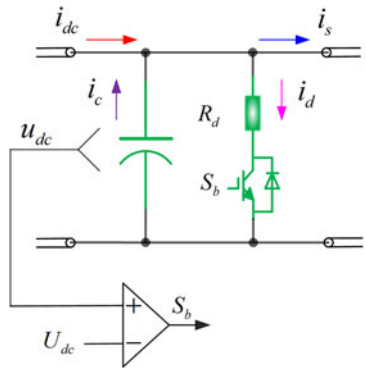

Fig. 10. Chopper circuit and its control scheme.

The commonly used chopper circuit and its control scheme is shown in Fig. 10. The chopper circuit comes into effect when u_{dc} exceeds a certain threshold value.

According to (17) and (18), the dynamic behaviors of RSG's rotor and SSG's capacitor are first-order differential equations with a similar pattern; T and i, Ω and u_{dc}, T_{a} and i_{c} are corresponding variables (see Fig. 9). Therefore, the energy transfer process (also the electromechanical transient process) of RSG and SSG can be rewritten in the generic form as

$$T_{\mathrm{J}} \frac{dx}{dt} = P_{\mathrm{in}} - P_{\mathrm{e}} \tag{20}$$

where, P_{in} and P_{e} are the input power of the energy transfer medium (rotor in RSG and dc capacitor in SSG) and the output electromagnetic power of SG (RSG/SSG), respectively; T_{J} is the inertia coefficient of electromechanical transient process.

Obviously, the energy transfer process keeps its equilibrium when $P_{\rm in}$ balances $P_{\rm e}$. The control strategies of SSG (including the fundamental and additional control) aim to achieve power balance, as well as the safe and stable operation of the overall energy transfer process by controlling the prime mover power and/or the output electromagnetic power. Hence, the electromechanical transient process illustrated in (20) is the foundation of SSG dynamic behavior as well as stability analysis.

In the following section, the electromechanical transient process of SSG is analyzed and the corresponding mathematical model, i.e., the swing equation is built. Results suggest that SSG and RSG can be expressed in uniform physical models, and the dynamic behaviors can be described by the same generalized mathematical model.

IV. Swing Equation of SSG

A. Normalization of SSG Swing Equation

By choosing the rated capacitor voltage $U_{\rm dc}$ as the SSG dc-side base voltage $U_{\rm dcB}$, the base current of dc-side is

$$I_{\rm B} = \frac{S_{\rm B}}{U_{\rm dcB}} = \frac{P_{\rm B}}{U_{\rm dc}}. \tag{21}$$

It is

$$i_{\rm c} = C\frac{du_{\rm dc}}{dt} = \frac{\frac{1}{2}CU_{\rm dc}^2}{\frac{1}{2}CU_{\rm dc}^2}\cdot C\cdot\frac{du_{\rm dc}}{dt} = \frac{2E_K}{U_{\rm dc}^2}\frac{du_{\rm dc}}{dt}. \tag{22}$$

By substituting (22) into (19) and dividing both sides of the equation by base value of dc-side current $I_{\rm B}$, we get

$$\begin{aligned}\frac{2E_{\rm K}}{I_{\rm B}U_{\rm dc}}\frac{d\left(\frac{u_{\rm dc}}{U_{\rm dc}}\right)}{dt} &= \frac{2E_{\rm K}}{P_{\rm B}}\frac{du_{\rm dc}^*}{dt}\\ &= \frac{i_{\rm dc}}{I_{\rm B}} - \frac{i_{\rm s}}{I_{\rm B}} - \frac{i_{\rm d}}{I_{\rm B}}\\ &= i_{\rm dc}^* - i_{\rm s}^* - i_{\rm d}^*.\end{aligned} \tag{23}$$

We designate the equivalent inertia coefficient of SSG as $T_{\rm J}$. It is

$$T_{\rm J} = \frac{2E_{\rm K}}{P_{\rm B}}. \tag{24}$$

Accordingly, (23) can be rewritten as

$$T_{\rm J}\frac{du_{\rm dc}^*}{dt} = i_{\rm dc}^* - i_{\rm s}^* - i_{\rm d}^* \tag{25}$$

which is the normalized virtual swing equation of SSG.

Let $i_{\rm c}^* = 1$. Hence

$$\begin{aligned}\tau &= \int_0^\tau dt = \int_0^\tau \frac{T_{\rm J}}{i_{\rm dc}^* - i_{\rm s}^* - i_{\rm d}^*}du_{\rm dc}^*\\ &= \int_0^\tau \frac{T_{\rm J}}{i_{\rm c}^*}du_{\rm dc}^* = T_{\rm J}\int_0^1 du_{\rm dc}^* = T_{\rm J}.\end{aligned} \tag{26}$$

From (26), it is obvious that $T_{\rm J}$ is the time duration required for dc capacitor voltage $u_{\rm dc}$ to be raised from 0 to its nominal value $U_{\rm dc}$ (i.e., $u_{\rm dc}^* = 1$), with rated charging current $I_{\rm B}$ ($i_{\rm c}^* = 1$). This gives the physical interpretation of the equivalent inertia coefficient $T_{\rm J}$ and reflects the intrinsic charging/discharging capacity of SSG.

In addition, (25) can be expressed in terms of power as

$$T_{\rm J}\frac{du_{\rm dc}^*}{dt} = \frac{P_{\rm dc}^*}{u_{\rm dc}^*} - \frac{P_{\rm s}^*}{u_{\rm dc}^*} - \frac{P_{\rm d}^*}{u_{\rm dc}^*}. \tag{27}$$

As a simplified assumption, $u_{\rm dc}^*$ is kept constant 1 in that the variations of $u_{\rm dc}$ are small with capacitor voltage control. Besides, conclusions will be unaffected with this assumption in the cases of stability investigation and instability mechanism analysis, hence this simplification is commonly utilized in RSG dynamic analysis.

Consequently, the standard model of swing equation in SSG can be obtained from (27), by considering the relationship between the power angle δ and grid angular frequency ω, as (in p.u.)

$$\begin{cases}\dfrac{d\delta}{dt} = (\omega - 1)\,\omega_{\rm s}\\ T_{\rm J}\dfrac{du_{\rm dc}}{dt} = P_{\rm dc} - P_{\rm s} - P_{\rm d}.\end{cases} \tag{28}$$

By substituting the linearized SSG electromagnetic power in (1) into (28) and assuming that the input power of prime mover keeps constant ($\Delta P_{\rm dc} = 0$), standard dynamic equation of SSG can be obtained as

$$\begin{cases}\dfrac{d\Delta\delta}{dt} = \Delta\omega\\ T_{\rm J}\dfrac{d\Delta u_{\rm dc}}{dt} = -T_{\rm S}'\Delta\delta - T_{\rm D}'\Delta u_{\rm dc}\end{cases} \tag{29}$$

where,

$$\begin{cases}T_{\rm J} = \dfrac{2E_{\rm K}}{P_{\rm B}}\\ T_{\rm S}' = 1.5KU_{\rm g}\\ T_{\rm D}' = \dfrac{1}{R_{\rm d}}.\end{cases} \tag{30}$$

It is evident that the swing equations of RSG and SSG are coherent in form with different state variables (ω and $u_{\rm dc}$). Further study is needed about the relationship between ω, δ, and $u_{\rm dc}$ to determine whether ω in RSG is the counterpart of $u_{\rm dc}$ in SSG.

B. Modeling and Investigating the Inherent Relationship Between Frequency, Power Angle, and DC Capacitor Voltage

From the phasor diagram illustrated in Fig. 5, it is

$$i_{\rm d} = \frac{U_{\rm s}}{X}\sin\delta. \tag{31}$$

For the basic SSG control scheme (see Fig. 6), the bandwidth of inner current loop is designed overwhelmingly large such that the inner-loop transient is negligible compared with the outer loop. Consequently, the inner-loop current in Fig. 6(b) yields

$$i_{\rm d} = i_{\rm d}^* = -\left(K_{\rm p} + \frac{K_{\rm i}}{s}\right)(U_{\rm dc} - u_{\rm dc}) \tag{32}$$

where $K_{\rm p}$ and $K_{\rm i}$ are proportional and integral gains of the outer voltage loop, respectively.

By combining (31) and (32), the relationship between δ and u_{dc} yields

$$\frac{U_{\mathrm{s}}}{X}\sin\delta = -\left(K_{\mathrm{p}} + \frac{K_{\mathrm{i}}}{s}\right)\left(U_{\mathrm{dc}} - u_{\mathrm{dc}}\right). \tag{33}$$

Generally, only the incremental relationship is considered for stability analysis. Accordingly, by linearizing (33), we have

$$sK\Delta\delta = \left(sK_{\mathrm{p}} + K_{\mathrm{i}}\right)\Delta u_{\mathrm{dc}}. \tag{34}$$

By manipulating (34) and substituting $\Delta\omega$ for $s\Delta\delta$, we have

$$\frac{K}{\Delta u_{\mathrm{dc}}} = \frac{K_{\mathrm{p}}}{\Delta\delta} + \frac{K_{\mathrm{i}}}{\Delta\omega}. \tag{35}$$

It is apparent from the linearized model in (35) that u_{dc} in SSG cannot be simply related to ω in RSG. To relate the physical meanings of ω, δ, and u_{dc}, the effects of P, I, and PI regulators are discussed respectively.

For P regulator, $K_{\mathrm{i}} = 0$ and the linearized model between δ and u_{dc} can be obtained as

$$\Delta\delta = \frac{K_{\mathrm{p}}}{K}\Delta u_{\mathrm{dc}}. \tag{36}$$

Similarly, for I regulator ($K_{\mathrm{p}} = 0$), the linearized model between ω and u_{dc} is

$$\Delta\omega = \frac{K_{\mathrm{i}}}{K}\Delta u_{\mathrm{dc}}. \tag{37}$$

It is obvious from (35) that with PI regulator, the control of u_{dc} indicate the simultaneous control of ω and δ.

Besides, the incremental relationship between ω and δ can be readily obtained from Fig. 5 as

$$\frac{d\Delta\delta}{dt} = \Delta\omega. \tag{38}$$

We can summarize from (35)–(38) that Δu_{dc} is proportional to $\Delta\delta$ under the effect of P regulator, i.e., in this case u_{dc} in SSG is the counterpart of δ in RSG, thus the control of u_{dc} equates the control of δ. In the case of I regulator, Δu_{dc} is proportional with the time derivative of $\Delta\delta$, i.e., $\Delta\omega$, in this case u_{dc} in SSG corresponds to ω in RSG and the control of u_{dc} is coherent with the control of ω.

C. Phillips–Heffron Model of SSG

Phillips–Heffron model, which clearly indicates the linearized relationship between physical quantities, is one of the main approaches to system analysis and control. In this section, Phillips–Heffron model of SSG is established in a similar pattern with that of RSG. First, substituting $s\Delta\delta$ by $\Delta\omega$, (34) can be rewritten as

$$\Delta\omega = \frac{1}{K}\left(sK_{\mathrm{p}} + K_{\mathrm{i}}\right)\Delta u_{\mathrm{dc}}. \tag{39}$$

Combining (29) and (39), the Phillips–Heffron model of SSG can be obtained as shown in Fig. 11(a). Compared with the model of RSG [see Fig. 11(b)], the model of SSG shares the same structure except for the encircled area and system parameters.

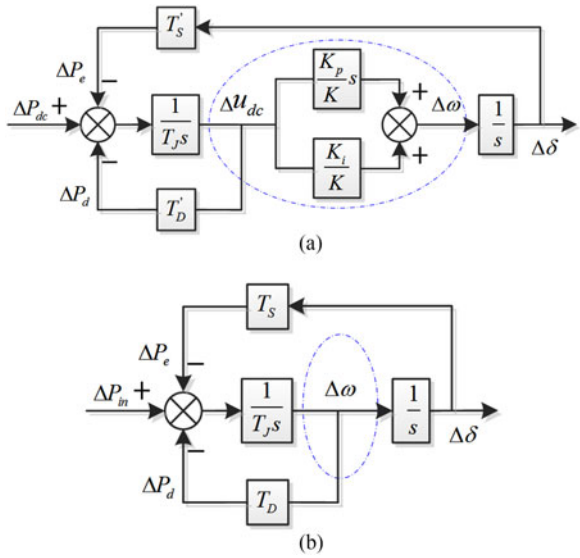

Fig. 11. Phillips–Heffron model of (a) SSG and (b) RSG.

Rewriting (29) in Laplace domain and combining with (39), we have

$$\begin{cases} s\Delta\delta = \Delta\omega \\ T_{\mathrm{J}}s^2\Delta\delta = -\left(\dfrac{K_{\mathrm{p}}}{K}T_{\mathrm{S}}' + T_{\mathrm{D}}'\right)s\Delta\delta - \dfrac{K_{\mathrm{i}}}{K}T_{\mathrm{S}}'\Delta\delta. \end{cases} \tag{40}$$

By substituting $s\Delta\delta$ by $\Delta\omega$ and rearranging, the standard swing equation of SSG can be obtained as

$$\begin{cases} \dfrac{d\Delta\delta}{dt} = \Delta\omega \\ T_{\mathrm{J}}\dfrac{d\Delta\omega}{dt} = -T_{\mathrm{S}}\Delta\delta - T_{\mathrm{D}}\Delta\omega \end{cases} \tag{41}$$

where, T_{J}, T_{S}, and T_{D} denote the equivalent inertia, synchronizing and damping coefficients of RSG, respectively.

Similarly, the Phillips–Heffron model is also identical to that of RSG [see Fig. 11(b)], where T_{J}, T_{D}, and T_{S} of SSG yield

$$\begin{cases} T_{\mathrm{J}} = \dfrac{2E_{\mathrm{K}}}{P_{\mathrm{B}}} = \dfrac{CU_{\mathrm{dc}}^2}{S_{\mathrm{B}}} \\ T_{\mathrm{D}} = \dfrac{K_{\mathrm{p}}}{K}T_{\mathrm{S}}' + T_{\mathrm{D}}' = 1.5K_{\mathrm{p}}U_{\mathrm{g}} + \dfrac{1}{R_{\mathrm{d}}} \\ T_{\mathrm{S}} = \dfrac{K_{\mathrm{i}}}{K}T_{\mathrm{S}}' = 1.5K_{\mathrm{i}}U_{\mathrm{g}}. \end{cases} \tag{42}$$

Obviously, (42) suggests that the damping effect, which provides SSG with the immunity to external disturbances by damping oscillations, is generated by chopper circuit and P regulator. The I regulator provides SSG with the synchronization ability which helps SSG to work at the desired operating point. It should be noted that the VSG scheme plays a role of P regulator and, therefore, can only change the damping effect instead of inertia, from a perspective of the developed SSG model.

If K_{p} and K_{i} are both positive, T_{J}, T_{S}, and T_{D} will be positive simultaneously, indicating that SSG is equipped with certain inertia, damping, and synchronizing ability. This case corresponds

to the negative feedback control. Positive values of K_{p} and K_{i} indicate positive inertia, damping and synchronizing abilities, as well as stability of SSG, yet further investigation is still needed for analyzing the stability margin, influential factors as well as principles.

V. Analysis and Criterion of SSG Stability

The electromechanical dynamic process and the stability behavior of SSG are discussed, thus the small-signal and transient stability criteria are established. The damping effect related to the structure and chopper circuit is too small to be considered. Accordingly, the output power P_{s} equates the prime mover power P_{dc} in steady state [see Fig. 12(a)], hence, operating points **a** and **b** are present, satisfying power balance. It can be readily seen that the power balance of SSG cannot be maintained when P_{dc} exceeds P_{smax} (which corresponds to the critical point with δ equal to $90°$), causing instability of SSG.

In the following parts, the dynamic processes at operating points **a** and **b** are analyzed separately with respect to small-signal and transient stability in order to analyze the ability and principle for SSG to maintain its stability.

A. Small-Signal Stability Criterion

Small-signal stability is the ability to maintain synchronism under small disturbances. In this case, only operating point **a** is able to operate stably, while operating point **b** is unstable [see Fig. 12(a)]. The detailed analysis is given below.

1) Point **a***:* Assume that a positive disturbance $\Delta\delta$ is imposed on power angle δ_{a} such that the new power angle becomes $\delta_{\mathrm{a}\prime}$. In this case, P_{s} is bigger than P_{dc}, hence the dc-side capacitor will discharge and u_{dc} will decrease. According to (36), δ decreases with the aid of PI regulator, and will return to equilibrium point **a** [see Fig. 12(b)] with the damping and synchronizing ability provided by PI regulator. Likewise, a negative disturbance $\Delta\delta$ will cause δ change from δ_{a} to $\delta_{\mathrm{a}\prime\prime}$ where P_{dc} is greater than P_{s} and the capacitor will charge, consequently δ is going to increase. During the negative feedback processes above, δ will eventually return to the initial steady-state point δ_{a} via the system control, hence, the operating point **a** is small-signal stable. Similarly, the operating region on the left part of critical point is small-signal stable.

2) Point **b***:* The small-signal stability at point **b** is completely different from that at point **a**. Similarly, assuming a positive $\Delta\delta$ is imposed on δ_{b}, such that δ increases to $\delta_{\mathrm{b}\prime}$. Accordingly, P_{dc} is greater than P_{s}, hence, the capacitor will charge and u_{dc} will increase, causing δ increasing. However, this case leads to a further decrease of P_{s}, causing the capacitor charging and u_{dc} increase, hence, δ will keep increasing as a chain reaction [see Fig. 12(c)]. Obviously, a positive power angle disturbance will introduce a positive feedback, and thus, nonoscillatory instability. On the contrary, if δ is changed from δ_{b} to $\delta_{\mathrm{b}\prime\prime}$ with a negative angle disturbance, P_{dc} is smaller than P_{s} and the capacitor discharges, leading to decrease of δ and further increase of P_{s}, consequently capacitor discharges with higher speed and δ continuously decreases until δ lies in the stable region. Afterward, the behavior of δ corresponds to the case in Fig. 12(b), i.e., SSG eventually stabilizes at the stable point δ_{a}. Therefore, the system operating at point **b** will either lose its stability or regain stability by moving to point **a**, i.e., point **b** is small-signal unstable. Similarly, the operating region on the right part of critical point is small-signal unstable.

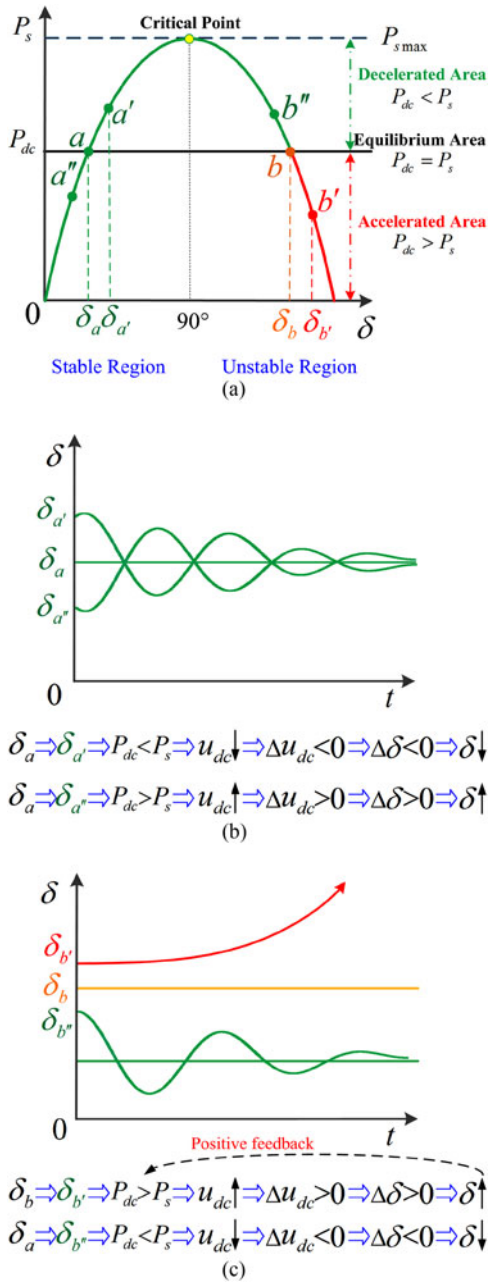

Fig. 12. Illustration of SSG's small-signal stability. (a) Power-angle curve, (b) response at point **a** and (c) response at point **b**.

Integrating the above two situations, it is obvious that when SSG operates on the left of critical point (i.e., $\delta < 90°$), the output power will increase with respect to the increase of δ (and vice versa), i.e., system is small-signal stable when $dP_s/d\delta > 0$. Similarly, when SSG operates on the right of critical point (i.e., $\delta > 90°$), the output power will increase with the decrease of δ (and vice versa), i.e., system is small-signal unstable when $dP_s/d\delta < 0$.

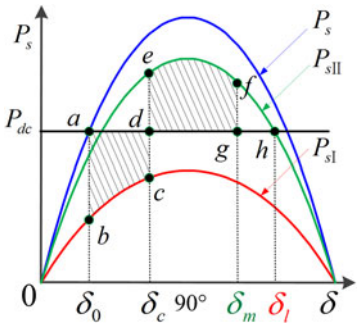

Fig. 13. Illustration of SSG power angle during transient.

Therefore, the small-signal stability criterion of SSG is given by

$$\frac{dP_{\rm s}}{d\delta} = \frac{3}{2}\frac{U_{\rm s}U_{\rm g}}{X}\cos\delta > 0. \tag{43}$$

Obviously, (43) reveals a clear physical interpretation that SSG is small-signal stable only when the output power changes in the same trend with power angle (i.e., system is synchronized). Furthermore, δ is proportional with $u_{\rm dc}$ according to (36), hence, the small-signal stability of SSG requires the same change direction of output power and capacitor voltage. Increase in capacitor voltage suggests residual power, accordingly more power needs to be generated by SSG such that power balance is achieved in electromechanical process, otherwise SSG will lose its stability.

B. Transient Stability Criterion

Transient stability is the ability of SSG to maintain synchronism when subjected to a severe transient disturbance. The system response involves large excursions of capacitor voltages and is influenced by the nonlinear power-angle relationship. Stability depends on both the initial operating state and the severity of disturbance. Usually, the system is altered so that the post-disturbance steady-state operation differs from that prior to the disturbance, as shown in Fig. 13. The power angle behavior during transient is analyzed in detail as follows.

1) Steady-State Operation at Point **a***:* Power balance (i.e., $P_{\rm dc} = P_{\rm s}$) is achieved when SSG operates at point **a** (which is inside the small-signal stability region), hence, SSG is able to work stably under small disturbances. The power angle in this case is denoted as δ_0 and the blue curve ($P_{\rm s}$) represents the power-angle curve.

2) During Fault: When a fault (e.g., low-voltage fault) occurs, the power-angle curve drops from $P_{\rm s}$ to $P_{\rm sI}$ (see Fig. 13, red curve). It's noted that the offset is larger if the fault is more severe. Accordingly, the instantaneous output power will fall (or increase with another fault type) to point **b**. In this case, $P_{\rm dc} > P_{\rm s}$ and the dc-side capacitor will charge, leading to continuous increase of $u_{\rm dc}$ and δ. More power is generated to balance the charging power of capacitor.

3) After Fault Clearing: Assuming that fault is detected and instantaneously cleared when δ increases to $\delta_{\rm c}$, after that the power angle curve elevated from $P_{\rm sI}$ to $P_{\rm sII}$ (see Fig. 13, green curve) or $P_{\rm s}$ if normal system operation can be retrieved after the fault is cleared. At the time instant when fault is cleared, the instantaneous output power rises to point **e** with $\delta_{\rm c}$ at that time. At the same time, $P_{\rm dc} < P_{\rm s}$, and hence, the dc-side capacitor will discharge, leading to continuous decrease of $u_{\rm dc}$. However, $u_{\rm dc}$ is still greater than its nominal value $U_{\rm dc}$, leading to continuous increase of δ such that more power can be generated to accelerate capacitor discharging.

When δ increases to $\delta_{\rm m}$, $u_{\rm dc}$ drops to its nominal value $U_{\rm dc}$. After that δ will continuously decrease to generate less power, thus, lower the speed of capacitor discharging. Hence, $\delta_{\rm m}$ is the extreme position of power angle during the transient.

It is evident that $\delta_{\rm m}$ must be strictly smaller than the limit power angle $\delta_{\rm l}$, otherwise a positive feedback is formed and SSG will lose its stability in a similar pattern as $\delta_{\rm b\prime}$ in Fig. 12(a). Therefore, the transient stability criterion is given by $\delta_{\rm m} \le \delta_{\rm l}$.

According to the analysis above, dc capacitor will absorb extra energy and charge during the fault, furthermore the increased stored energy equates the value of accelerating area S_+ (encircled by abcd), i.e.,

$$S_+ = \int_{\delta_0}^{\delta_{\rm c}} (P_{\rm dc} - P_{\rm sI})\, d\delta. \tag{44}$$

Similarly, after the fault is cleared, the capacitor will release the extra energy during charging in order to return to its normal state. The released energy, which equates the decelerating area S_- (enclosed by defg), can be expressed as

$$S_- = \int_{\delta_{\rm c}}^{\delta_{\rm m}} (P_{\rm sII} - P_{\rm dc})\, d\delta. \tag{45}$$

Hence, the maximum decelerating area available is given by

$$S_{-\max} = \int_{\delta_{\rm c}}^{\delta_{\rm l}} (P_{\rm sII} - P_{\rm dc})\, d\delta. \tag{46}$$

Obviously, the absorbed energy during acceleration must be completely released in order to bring the capacitor voltage back to normal, otherwise the energy stored in capacitor will keep increasing and the SSG will eventually lose its stability. Therefore, the transient stability criterion of the SSG can be described as $S_+ \le S_{-\max}$.

It is apparent that clearing the fault timely is of paramount importance in keeping the transient stability of SSG, elsewise the dc capacitor will be charged with too much energy that cannot be released thoroughly before the limit power angle $\delta_{\rm l}$ is achieved and the system is unstable. Therefore, assuming the critical power angle at which the fault can be successfully cleared and SSG transient stability can be guaranteed is $\delta_{\rm cm}$, it is

$$\int_{\delta_0}^{\delta_{\rm cm}} (P_{\rm dc} - P_{\rm sI})\, d\delta = \int_{\delta_{\rm cm}}^{\delta_{\rm l}} (P_{\rm sII} - P_{\rm dc})\, d\delta. \tag{47}$$

Considering that $P_{\rm sI} = P_{\rm sI\,max}\sin\delta$ and $P_{\rm sII} = P_{\rm sII\,max}\sin\delta$, the critical power angle $\delta_{\rm cm}$ for fault clearing can be expressed as

$$\cos\delta_{\rm cm} = \frac{P_{\rm dc}\,(\delta_{\rm l} - \delta_0) + P_{\rm sII\,max}\cos\delta_{\rm l} - P_{\rm sI\,max}\cos\delta_0}{P_{\rm sII\,max} - P_{\rm sI\,max}}. \tag{48}$$

If δ is greater than $\delta_{\rm cm}$ at the instant of fault clearing, SSG will lose its synchronization, and thus, stability inevitably. On

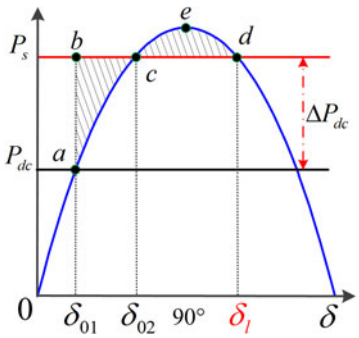

Fig. 14. Influence of input power ramp rate on SSG transient stability.

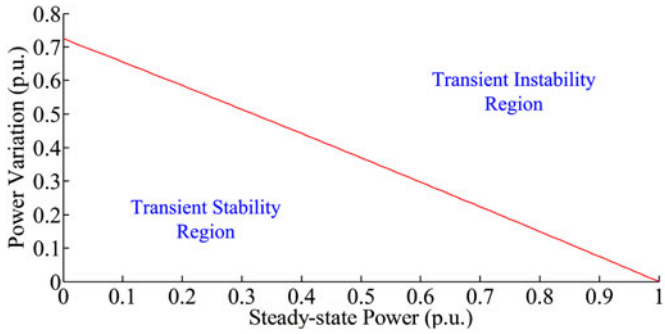

Fig. 15. Relationship between $P_{\rm dc}$ and $\Delta P_{\rm dc}$ in critical state of transient stability.

the contrary, transient stability maybe ensured if fault is cleared before power angle reaches $\delta_{\rm cm}$.

C. Power Variation Criteria of Renewable Energy

Power variation is a critical issue related to the integration of directly grid-tied renewable energy, which depresses the power quality and also may result in dynamic instability in extreme cases such as sudden large power variation. In this sense, the power variation in renewable energy generation system must be limited, which is analyzed in Fig. 14.

In normal condition, the SSG operates stably at point **a**. A disturbance $\Delta P_{\rm dc}$ is introduced, leading to the change of input power to $P_{\rm dc}+\Delta P_{\rm dc}$ as well as steady-state point to **c** (with power angle δ_{02}). According to the transient stability criterion, the maximum power variation occurs when the energy releasing process (enclosed by cde) of capacitor (with extra energy enclosed by abc during charging) terminates at limit power angle $\delta_{\rm l}$. Accordingly

$$\int_{\delta_{01}}^{\delta_{02}} \left(P_{\rm dc}+\Delta P_{\rm dc}-P_{\rm s}\right) d\delta = \int_{\delta_{02}}^{\delta_{\rm l}} \left(P_{\rm s}-P_{\rm dc}-\Delta P_{\rm dc}\right) d\delta. \tag{49}$$

If per-unit values, taking $P_{s\,\max}$ as the base value, are utilized for $P_{\rm dc}$ and $\Delta P_{\rm dc}$, then $\sin\delta_{01}=P_{dc}$ and $\sin\delta_l=P_{dc}+\Delta P_{dc}$. Consequently, (49) can be rewritten as

$$\begin{aligned}&\left(P_{\rm dc}+\Delta P_{\rm dc}\right)\arcsin\left(P_{\rm dc}\right)+\cos\left[\arcsin\left(P_{\rm dc}\right)\right]\\ =\ &\left(P_{\rm dc}+\Delta P_{\rm dc}\right)\left[\pi-\arcsin\left(P_{\rm dc}+\Delta P_{\rm dc}\right)\right]\\ &-\cos\left[\arcsin\left(P_{\rm dc}+\Delta P_{\rm dc}\right)\right].\end{aligned} \tag{50}$$

Obviously, (50) illustrates the relationship between the input power $P_{\rm dc}$ and its maximum variation $\Delta P_{\rm dc}$ for SSG in the critical state of transient stability. The numerical results are given in Fig. 15.

According to Fig. 15, it is apparent that the allowed maximum $\Delta P_{\rm dc}$ and stability margin decreases with the increase of steady-state point $P_{\rm dc}$. Obviously, the transient stability is guaranteed in region below the curve, and system is transient unstable in the above region. Hence, this curve serves as the transient stability boundary of renewable energy with power variation.

Besides reserving sufficient stability margin, the maximum power variation of renewable energy should also be limited. Furthermore, the limit varies with different operating point and can be designed according to the stability boundary in Fig. 15.

D. Dynamic Behavior and Stability Analysis of SSG

In the following parts, the dynamic behavior of the SSG with small disturbance is analyzed, meanwhile factors that influence the stability and the corresponding principles are discussed based on Fig. 16.

Small disturbances lead to an inevitable slight change of $u_{\rm dc}$, resulting in the variations of δ and output power of SSG. According to the conclusions of small-signal stability corresponding to Fig. 12, the left and right regions with respect to the critical power $P_{\max}$ correspond to the small-signal stable and instable region, respectively. Assume the original operation point of SSG is A, which will change to point B when steady state is obtained after disturbance. In the following parts, the effects of controller parameters, system parameters, and the steady-state point on SSG stability are analyzed in detail.

1) Effect of Control Parameters: The main control parameters are $K_{\rm p}$ and $K_{\rm i}$. Fig. 16(a) illustrates the effect of different parameters with respect to the same disturbance $\Delta P_{\rm dc}$, leading to capacitor charging, and thus, increase of $u_{\rm dc}$, accordingly the steady-state point moves from A to B. In a same time duration, δ will increase from δ_0 to δ_1 with small values of $K_{\rm p}$ and $K_{\rm i}$, and will increase significantly to δ_2 (which is closer to the new stable point B) with larger parameters.

According to (42), the larger values of $K_{\rm p}$ and $K_{\rm i}$, the stronger synchronization and damping abilities. With the increase of equivalent damping coefficient $T_{\rm D}$, damping ability of power angle oscillations will be stronger, thus $u_{\rm dc}$ will come into steady state with quicker dynamic response. Besides, a larger value of system equivalent synchronization coefficient $T_{\rm S}$ indicates stronger steady-state control ability (i.e., synchronizing ability) of $u_{\rm dc}$ and, thus, $u_{\rm dc}$ will be stabilized at its reference value $U_{\rm dc}$ with quick dynamic and virtually no error. Classical control theory believes that $K_{\rm i}$ records the historical data of $\Delta u_{\rm dc}$ and provides SSG with the ability in eliminating steady-state errors. Apparently, the conclusions obtained via the SSG model and its stability analysis are coherent with the classical control theory.

However, larger $K_{\rm p}$ and $K_{\rm i}$ will also lead to possible instabilities. If $\Delta\delta$ is rather large with the improper PI parameters that the new power angle (e.g., δ_3) falls in the unstable region, SSG could lose its stability. Apparently, larger values of $K_{\rm p}$ and $K_{\rm i}$ are unfavorable for systems with small stability margin. A compromise has to be made between the system response speed and the stability when choosing controller parameters.

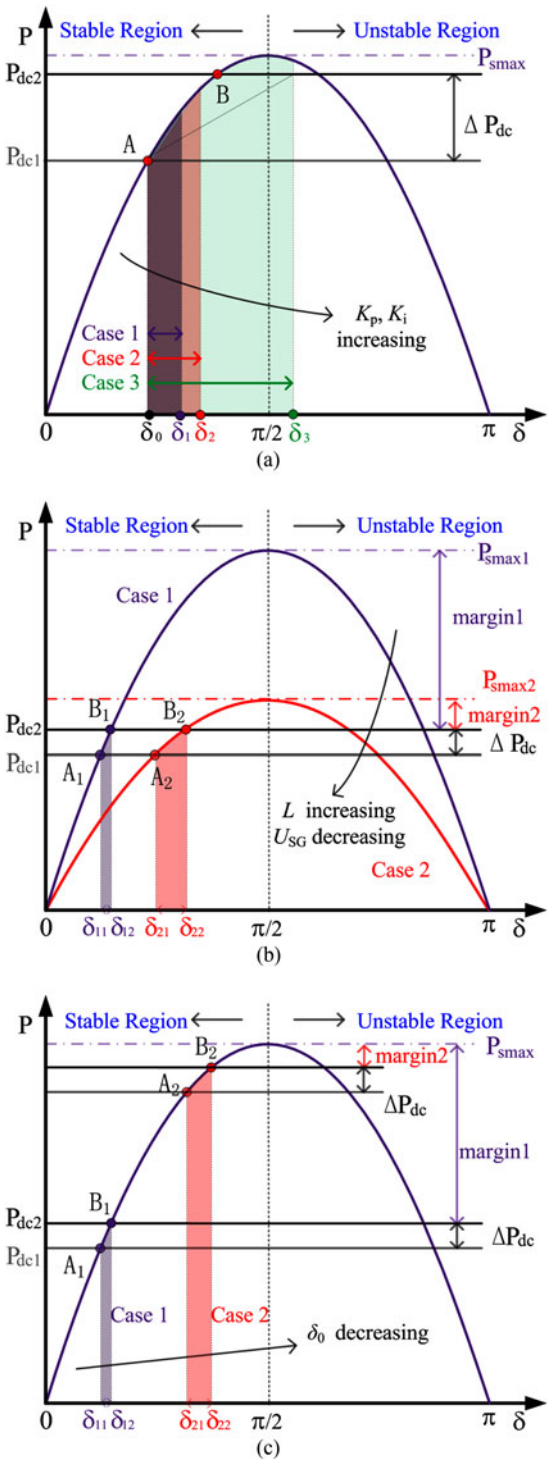

Fig. 16. Influence of (a) control parameters, (b) system parameters and (c) steady-state power angle δ_0 on SSG small-signal stability.

2) Effect of System Parameters: The system parameters are L and C. From Fig. 16(b), the change of δ is larger with greater L (from the purple curve to the red curve) on the condition of same ΔP. A small value of Δu_{dc} will lead to significant change of $\Delta\delta$ when L is large enough. Hence, it is evident that the larger inductance, the smaller the stability margin and weaker small-signal stability (as well as the transient stability) of SSG. The above results are coherent with the explanation from the classical theories of power system and power electronics. The conventional power system theory suggests that the value of the linking inductance indicates the correlation between two interconnection electric systems, i.e., large values of linking inductance suggests loose electric connections and worse stabilities, and vice versa. Similar conclusions can also be obtained from the viewpoint of impedance analysis based stability theory in power electronics system [20], [21].

3) Effect of Operating Point: The parameter K is determined by U_{s} and δ_0, i.e., it contains the information of the stable point of SSG. The effect of U_{s}, which lowers the maximum output power P_{emax} and system stability margin, can be analyzed similarly as the case with L. From Fig. 16(b), $\Delta\delta$ is smaller with larger U_{s} (the case of purple curve) on the condition of same ΔP, and this effect is beneficial for system stability. Therefore, increasing the internal voltage improves not only the ability of power transfer but also the stability of SSG. The effect of δ_0 is illustrated in Fig. 16(c). For the same ΔP, the change of $\Delta\delta$ increases with the stable power angle δ_0 (which increases from the purple to the red region), and this result is harmful to the system stability. It is evident that when δ_0 lies far from the unstable region, the stability margin will be larger and the small-signal stability will be better, coherent with the conclusions obtained from Fig. 15. However, too small δ_0 will lead to waste of the designed power capacity, hence the system is not economical. Accordingly, two contradictory factors, i.e., system stability margin and power capacity utilization, have to be both considered in the operation point design.

E. Main Conclusion Summary

Based on the developed SSG model and its related analysis, following main conclusions are obtained:

1) The inertia coefficient of the SSG is proportional to the dc capacitance as well as capacitor voltage; the damping and synchronizing ability are dependent on the proportional and integral gain of dc capacitor voltage loop, respectively. The larger values of control parameters, the better regulation ability of dc capacitor voltage, thus better stability of the SSG.
2) The linking inductance reflects the electric connection property between SSG and power grid, i.e., larger linking inductance indicates weaker connection, and thus, the weaker stability of the SSG. Increasing the virtual internal voltage and the dc-side capacitor voltage can enhance not only the real-power transmission ability but the system stability.
3) The larger power angle (i.e., the operating point is close to the limit), the smaller stability margin system will have, and thus, the weaker system stability. For renewable energy generation systems, the range of power variation should be limited to avoid large deviation of steady-state operating point or, even worse, system instability.
4) Increasing the virtual internal voltage and the dc-side capacitor voltage of SSG will increase the hardware costs notably; if the steady-state operating point is designed to a small value, the capacity utilization rate will be too low.

TABLE III
PARAMETERS FOR SIMULATION

Parameters	Values
Grid Phase Voltage	220 V / 50 Hz
Chopping Frequency	10 kHz
DC-side Capacitor	3 mF / 750 V
Linking Inductance	2.0 mH
Proportional/Integral Gain of Outer Loop	40 / 100
Proportional/Integral Gain of Inner Loop	0.2 / 0.8

TABLE IV
PARAMETERS OF EXPERIMENTED SSG

Parameters	Values
Grid Phase Voltage	100 V / 50 Hz
Chopping Frequency	5 kHz
DC-side Capacitor	30 mF / 350 V
Linking Inductance	1.5 mH
Proportional/Integral Gain of Outer Loop	6 / 600
Proportional/Integral Gain of Inner Loop	0.16 / 0.26

Therefore, the operating point design has to compromise between system stability, capacity utilization, and hardware costs.

VI. SIMULATION & EXPERIMENTAL VERIFICATION

Simulations and experiments are performed based on the topology illustrated in Fig. 2, in which the prime mover of dc side is replaced by programmable dc source and the damper circuit is removed directly. The control structure takes the basic control scheme illustrated in Fig. 6. The main parameters are given in Tables III and IV.

A. Influence of Controller Parameters

Fig. 17(a) illustrates the influence mode of P controller on the damping characteristic of the SSG. K_{i} keeps 300 in all the cases. With the increase of K_{p}, the oscillation becomes smaller, indicating stronger damping effect. When $K_{\mathrm{p}} = 5$, the SSG operates in a critical damping state and system is characterized by both fast dynamic and small overshooting. It is apparent that larger K_{p} indicates a better damping ability; however, when the SSG stability margin is small, large K_{p} can lead to the movement of operating point to the unstable region. Fig. 17(b) shows the influence of I controller on system synchronization ability. K_{p} keeps 5 in these cases. With the increase of K_{i}, u_{dc} returns faster to the steady state (750 V), i.e., the greater K_{i}, the stronger regulation ability SSG has on the dc capacitor voltage, and the stronger synchronization ability SSG has. These results are coherent with the theoretical analysis, as shown in (42) and Fig. 16(a).

Besides, in the above cases when controller parameters are different, u_{dc} remained close to its rated value 750 V though the dynamic characteristics are not the same. This can be explained by the positive damping effect and synchronization capability provided by PI regulator, and hence, SSG is small-signal stable.

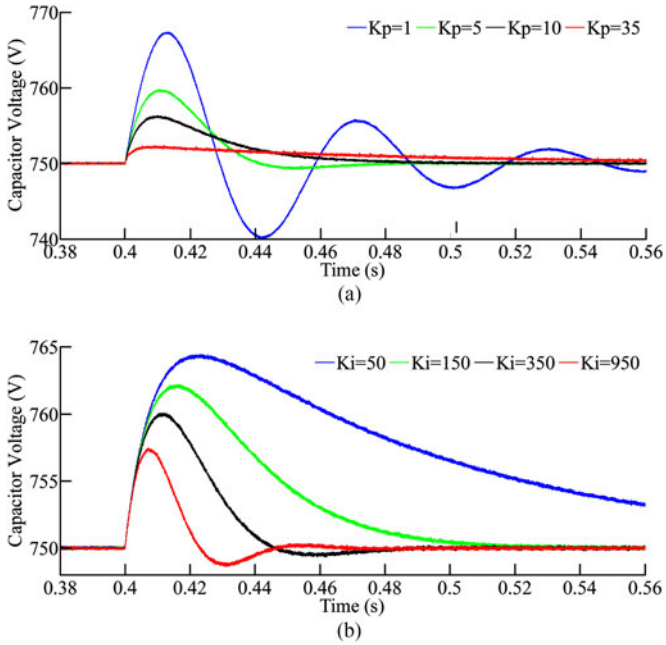

Fig. 17. Influence of (a) K_{p} and (b) K_{i} on dynamic behaviors and system stability.

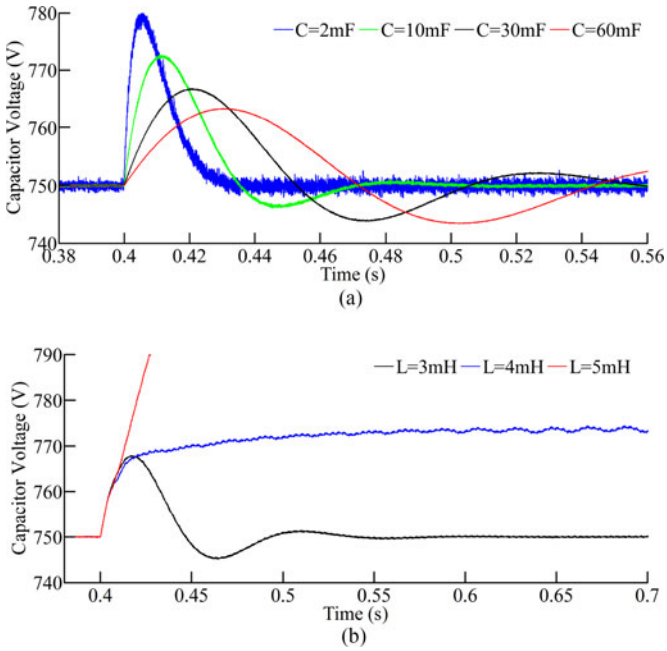

Fig. 18. Influence of system parameters. (a)Influence of dc-capacitance C on system inertia; (b) Influence of linking inductance L on system stability.

B. Influence of System Parameters

The system parameters include capacitance C and inductance L, which affect the inertia and stability of the SSG, respectively. Fig. 18 demonstrates the dynamic behavior of u_{dc} with respect to C and L changes. K_{p} and K_{i} are 2 and 200, respectively.

From Fig. 18(a), the oscillation of u_{dc} decreases with the increase of C, indicating better resistance of the SSG against external disturbances, i.e., higher inertia ability (T_{J}). This increase

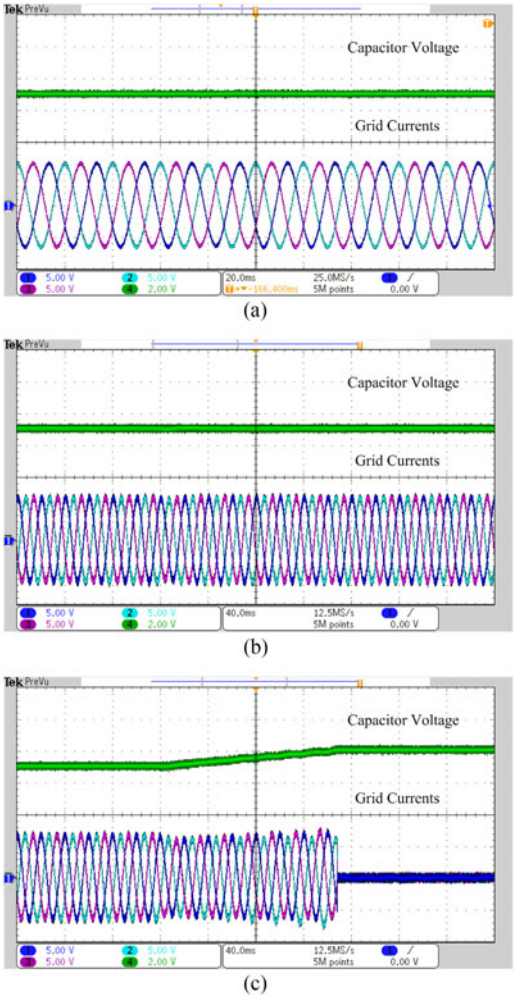

Fig. 19. Influence of linking inductance on the SSG stability. The linking inductance springs from 1.5 mH to (a) 2.0 mH (b) 2.5 mH and (c) 3.0 mH.

of system inertia is beneficial for capacitor voltage stabilization, avoiding overvoltage or even worse fault in the case of large external disturbances. This result is coherent with the theoretical one illustrated in (42). Besides, the increase of C results in a smoother capacitor voltage.

In normal operation, system is able to maintain stability under small disturbances. L springs to 3 mH/4 mH/5 mH at $t = 0.4$ s in order to study its influence on the overall system, and the simulation results are given in Fig. 18(b).

Fig. 18(b) reveals that the amplitude and time duration of capacitor voltage oscillation increases with larger L, i.e., the system stability is weakening. When L increases to 5 mH, the power injected by prime mover $P_{\rm dc}$ cannot be effectively transmitted and, thus, the dc capacitor can no longer balance the power. The extra charging power will cause continuous charging on the dc capacitor, leading to the intensive increase of $u_{\rm dc}$ and, thus, SSG loses its stability.

Experimental results in Fig. 19 demonstrate the influence of L on SSG transient stability. When L is 1.5 mH, $u_{\rm dc}$ keeps constant (350 V), and the system retains stability with small variations of inductance value during operation (e.g., L springs

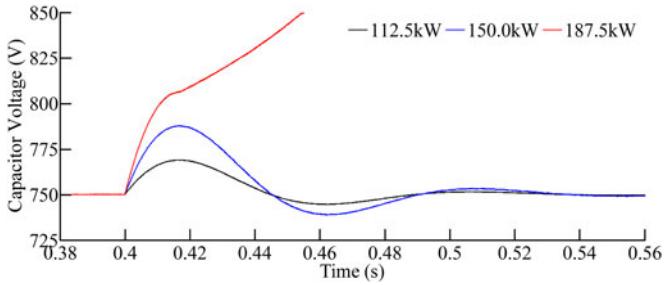

Fig. 20. Influence of steady-state points on system stability.

to 2.0 mH/2.5 mH), as shown in Fig. 19(a) and (b). However, when L continuously increases, the system transient stability will be worsen, thus stable operation cannot be ensured in the case of large inductance disturbance (see Fig. 19(c), L springs from 1.5 to 3.0 mH). The simulations and experiments provide corresponding results as the theoretical analysis, as illustrated in (43) and Fig. 16(b). Besides, it is noted that when $u_{\rm dc}$ exceeds 400 V, system operation is immediately terminated.

C. Influence of Power Variation

Fig. 20 shows the impact of the steady-state point on the dynamic stability of $u_{\rm dc}$. $P_{\rm dc}$ springs from 75 to 112.5 kW/150.0 kW/187.5 kW at 0.4 s. Simulation results indicate that the capacitor voltage oscillation becomes more intense, i.e., system stability gets weaker when system is close to the limit of operating point. When $P_{\rm dc}$ suddenly increases to 187.5 kW, the control system attempts to increase $u_{\rm dc}$ such that the unbalanced power can be absorbed, yet this process lasts merely for 3 ms, after which the voltage controller loses its capability and the capacitor voltage becomes unstable.

Besides, experimental results in Fig. 21 also verify the transient stability law illustrated in Fig. 15. From Fig. 21(a) and (b), stable operation can be maintained when $P_{\rm dc}$ jumps from 14 to 35 kW, yet it cannot when $P_{\rm dc}$ jumps to 42 kW. However, experiment result in Fig. 21(e) illustrates the stable operation as well as small-signal stability of SSG with 42 kW input power. Hence, the allowed deviation power for transient stability is between 21 and 28 kW when system is initially operating stably with 14 kW input power. Likewise, it can be readily seen from Fig. 21(c) and (d) that the allowed deviation power for transient stability is between 14 and 21 kW when $P_{\rm dc}$ is 21 kW. In the other case with 35 kW input power, the deviation power is between 7 and 14 kW [see Fig. 21(e) and (f)].

Obviously, both the simulation and experimental results prove that the allowed input power deviation decreases when SSG operating at higher power, which are coherent with the theoretical one, as illustrated in (50) and Fig. 15. Therefore, adequate stability margin must be ensured during normal system operation such that system can maintain its stability under common degree of disturbances. However, the larger the stability margin, the lower the SSG's capacity utilization. As a result, the stability and efficiency of device should be both taken into consideration in operation point design.

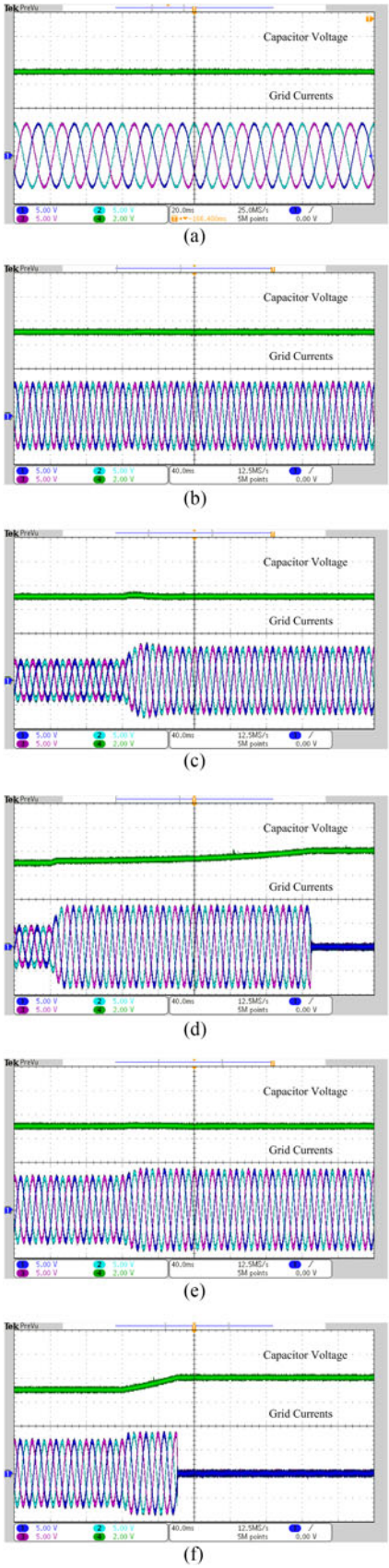

Fig. 21. Experimental results of system transient stability. The input power jumps (a) from 14 to 35 kW (b) from 14 to 42 kW (c) from 21 to 35 kW (d) from 21 to 42 kW (e) from kW to 42 kW and (f) from 35 to 49 kW, respectively.

VII. Conclusion

The electromechanical transient model and physical interpretation of SSG are presented to illustrate the inherent relationship and intrinsic differences between SSG and RSG, and results suggest that it is feasible to migrate the concepts, tools, and methods of RSG stability analysis to investigate the dynamic behaviors and stability issues of SSG. These results help to apply the well-developed theories and methods in conventional power system to the SSG, promoting the unity of RSG and SSG in both theories and methods for analyzing the dynamic behaviors and stability issues of the SSG, even the future SSG/RSG hybrid grid. Taking the stability issues as an example, the small-signal and transient stability of the grid-tied inverter are investigated clearly, and several important conclusions are obtained consequently.

Moreover, since RSG and SSG are inherently related, the stability analysis, parameters design, and control issues (including virtual inertia/damping control, frequency/voltage control, multimachine coordination operation, and so on) of SSG can be solved in a similar pattern as RSG. The above research helps to effectively bridge grid-tied inverter systems and conventional power systems. In this sense, the developed SSG model is beneficial for the clear cognizing of grid-tied inverters, as well as analyzing and designing the control strategies of SSG from the perspective of grid safety and stability. The SSG model can serve as the foundation of interdisciplinary research between power electronics and power system and, therefore, promote the grid-friendly integration of renewable energy to future grid.

References

[1] Y. S. Park, S. K. Sul, C. H. Lim, W.-C. Kim, and S.-H. Lee, "Asymmetric control of DC-link voltages for separate MPPTs in three-level inverters," *IEEE Trans. Power Electron.*, vol. 28, no. 6, pp. 2760–2769, Jun. 2013.

[2] Q. C. Zhong and G. Weiss, "Static synchronous generators for distributed generation and renewable energy," in *Proc. Power Syst. Conf. Expo.*, 2009, Mar. 2009, pp. 15–18.

[3] J. Yao, H. Li, Z. Chen, X. Xia, X. Chen, Q. Li, and Y. Liao, "Enhanced control of a DFIG-based wind-power generation system with series grid-side converter under unbalanced grid voltage conditions," *IEEE Trans. Power Electron.*, vol. 28, no. 7, pp. 3167–3181, Jul. 2013.

[4] Y. Zhou and H. Li, "Analysis and suppression of leakage current in cascaded-multilevel-inverter-based PV systems,"*IEEE Trans. Power Electron.*, vol. 29, no. 10, pp. 5265–5277, Oct. 2014.

[5] M. Amirabadi, A. Balakrishnan, H. A. Toliyat, and W. C. Alexander, "High-frequency AC-link PV inverter,"*IEEE Trans. Ind. Electron.*, vol. 61, no. 1, pp. 281–291, Jan. 2014.

[6] Q. C. Zhong, "Synchronverters: Inverters that mimic synchronous generators,"*IEEE Trans. Ind. Electron.*, vol. 58, no. 4, pp. 1259–1267, Apr. 2011.

[7] T. Shintai, Y. Miura, and T. Ise, "Oscillation damping of a distributed generator using a virtual synchronous generator,"*IEEE Trans. Power Del.*, vol. 29, no. 2, pp. 668–676, Apr. 2014.

[8] J.-H. Jeon, J.-Y. Kim, H.-M. Kim, S.-K. Kim, C. Cho, J.-M. Kim, J.-B. Ahn, and K.-Y. Nam, "Development of hardware in-the-loop simulation system for testing operation and control functions of micro-grid,"*IEEE Trans. Power Electron.*, vol. 25, no. 12, pp. 2919–2929, Dec. 2010.

[9] R. Majumder, "Some aspects of stability in microgrids,"*IEEE Trans. Power Syst.*, vol. 28, no. 3, pp. 3243–3252, Aug. 2013.

[10] D. J. Lee and L. Wang, "Small-signal stability analysis of an autonomous hybrid renewable energy power generation/energy storage system part I: time-domain simulations,"*IEEE Trans. Energy Conver.*, vol. 23, no. 1, pp. 311–320, Mar. 2008.

[11] F. Katiraei, M. R. Iravani, and P. W. Lehn, "Small-signal dynamic model of a micro grid including conventional and electronically interfaced distributed resources,"*IET Gener. Transm. Dis.*, vol. 1, no. 3, pp. 369–378, May. 2007.

[12] N. Pogaku, M. Prodanovic, and T. C. Green, "Modeling, analysis and testing of autonomous operation of an inverter based microgrid,"*IEEE Trans. Power Electron.*, vol. 22, no. 2, pp. 613–625, Feb. 2007.
[13] E. Barklund, N. Pogaku, M. Prodanovic, C. Hernandez-Aramburo, and T. C Green, "Energy management in autonomous micro-grid using stability contrained droop control of inverters,"*IEEE Trans. Power Electron.*, vol. 23, no. 5, pp. 2346–2352, May. 2008.
[14] A. I. M. Yasser and F. E. Ehab, "Adaptive decentralized droop controller to preserve power sharing stability of parallel inverters in distributed generation micro-grid,"*IEEE Trans. Power Electron.*, vol. 23, no. 6, pp. 2806–2816, Jun. 2008.
[15] X. Guo, Z. Lu, B. Wang, X. Sun, L. Wang, and J. M. Guerrero, "Dynamic phasors-based modeling and stability analysis of droop-controlled inverters for microgrid applications,"*IEEE Trans. Smart Grid*, vol. 5, no. 6, pp. 2980–2987, Nov. 2014.
[16] C. M. Wildrick and F. C. Lee, "A method of defining the load impedance specification for a stable distributed power system,"*IEEE Trans. Power Electron.*, vol. 10, no. 3, pp. 280–285, Mar. 1995.
[17] J. J. Liu, X. Feng, and F. C. Lee, "Stability margin monitoring for DC distributed power systems via perturbation approaches,"*IEEE Trans. Power Electron.*, vol. 18, no. 6, pp. 1254–1261, Jun. 2003.
[18] J. Kim, J. M. Guerrero, and P. Rodriguez, "Mode adaptive droop control with virtual output impedances for an inverter based flexible AC microgrid,"*IEEE Trans. Power Electron.*, vol. 26, no. 3, pp. 689–701, Mar. 2011.
[19] J. M. Guerrero, J. Matas, L. G. de Vicuna, M. Castilla, and J. Miret, "Decentralized control for parallel operation of distributed generation inverters using resistive output impedance,"*IEEE Trans. Ind. Electron.*, vol. 54, no. 2, pp. 994–1004, Apr. 2007.
[20] Z. Liu, J. J. Liu, W. H. Bao, and Y. L. Zhao, "Infinity-norm of impedance-based stability criterion for three-phase AC distributed power systems with constant power loads,"*IEEE Trans. Power Electron.*, vol. 30, no. 6, pp. 3030–3043, Jun. 2015.
[21] F. C. Liu, J. J. Liu, H. D. Zhang, and D. H. Xue, "Stability issues of Z+Z type cascade system in hybrid energy storage system (HESS),"*IEEE Trans. Power Electron.*, vol. 29, no. 11, pp. 5846–5859, Nov. 2014.
[22] F. M. A. Mohammadreza and F. E. S. Ehab, "Implementing virtual inertia in DFIG-based wind power generation,"*IEEE Trans. Power Syst.*, vol. 28, no. 2, pp. 1373–1384, Jun. 2013.
[23] Q. C. Zhong, P. L. Nguyen, and Z. Y. Ma., "Self-synchronized synchronverters: Inverters without a dedicated synchronization unit,"*IEEE Trans. Power Electron.*, vol. 29, no. 2, pp. 617–630, Feb. 2014.
[24] N. Soni, S. Doolla, and M. C. Chandorkar, "Improvement of transient response in microgrids using virtual inertia,"*IEEE Trans. Power Del.*, vol. 28, no. 3, pp. 1830–1838, Apr. 2013.
[25] M. Guan, W. Pan, J. Zhang, Q. Hao, J. Cheng, and X. Zheng, "Synchronous generator emulation control strategy for voltage source converter (VSC) Stations,"*IEEE Trans. Power Syst.*, vol. 30, no. 6, pp. 3093–3101, Nov. 2015.
[26] M. A. Torres, A. C. Lopes, L. A. Moran, and J. R. Espinoza, "Self-tuning virtual synchronous machine: A control strategy for energy storage systems to support dynamic frequency control,"*IEEE Trans. Energy Conver.*, vol. 29, no. 4, pp. 833–840, Apr. 2014.
[27] J. Alipoor, Y. Miura, and T. Ise, "Power system stabilization using virtual synchronous generator with alternating moment of inertia,"*IEEE J. Emerg. Sel. Topics Power Electron.*, vol. 3, no. 2, pp. 451–458, Apr. 2015.
[28] J. Driesen and K. Visscher, "Virtual synchronous generators," in *Proc. IEEE Power Energy Soc. Gen. Meeting.*, 2008, pp. 1–3.
[29] H. P. Beck and R. Hesse, "Virtual synchronous machine," in *Proc. 9th Int. Conf. Electr. Power Qual. Utilisation*, 2007, pp. 1–6.
[30] K. Visscher and S. W. H. De Haan, "Virtual synchronous machines for frequency stabilization in future grids with a significant share of decentralized generation," in*Proc. IET-CIRED Seminar SmartGrids Distrib.*, 2008, pp. 1–4.
[31] T. L. Vandoorn, B. Meersman, J. D. Kooning, and L. Vandevelde, "Analogy between conventional grid control and islanded microgrid control based on a global dc-link voltage droop,"*IEEE Trans. Power Del.*, vol. 27, no. 3, pp. 1405–1415, Jul. 2012.
[32] B. Wu, S. Li, Y. Liu, and K. Ma Smedley, "A new hybrid boosting converter for renewable energy applications," *IEEE Trans. Power Electron.*, vol. 31, no. 2, pp. 1203–1215, Feb. 2016.